CAV2009 – Paper No. 57

On pressure and temperature waves within a cavitation bubble

Peter F. Pelz
Technische Universität Darmstadt
Chair of Fluid Systems Technology
Darmstadt, Germany

Andreas Ferber
Technische Universität Darmstadt
Chair of Fluid Systems Technology
Darmstadt, Germany

ABSTRACT

The presented work is about the detailed pressure, temperature and velocity distribution within a plane, cylindrical and spherical cavitation bubble. The review of *Plesset & Prosperetti (1977)* and more recently the review of *Feng & Leal (1997)* describe the time behavior of the gas within a spherical bubble due to forced harmonic oscillations of the bubble wall. We reconsider and extend those previous works by developing from the conversation laws and the ideal gas law a boundary value problem for the distribution of temperature and velocity amplitude within the bubble. This is done for a plane, cylindrical, or spherical bubble. The consequences due to shape differences are discussed. The results show that an oscillating temperature boundary layer is formed in which the heat conduction takes places. With increasing dimensionless frequency, i.e. Péclet number, the boundary-layer thickness decreases and compression modulus approaches its adiabatic value. This adiabatic behaviour is reached at lower frequencies for the plane geometry in comparison with cylindrical and spherical geometry. This is due to the difference in the volume specific surface, which is 1, 2, 3 times the inverse bubble height/radius r_0 for the plane, cylindrical and spherical bubble respectively. For the plane bubble the analysis ends up in an eigenvalue problem with four eigenvalues and modes. The analytical result is not distinguishable from the numerical result for the plane case gained by a finite element solution. Interestingly if the diffusion time for the temperature distribution is of the order of the traveling time of a pressure wave no adiabatic behavior is observed. A parameter map for the different regimes is given. Since only the behavior of the gas within the bubble is considered the analysis is independent of the surface tension coefficient and the inertia of the surrounding liquid. For the plane bubble since there is no curvature there is no pressure change over the free surface. Despite of this a plane bubble is manly academic, since due to inertia the pressure within the fluid would have to be infinity if the liquid volume around the bubble is unbounded.

INTRODUCTION

The concern of the presented work is to lead to a better understanding what happens on the interior side of an oscillating plane, cylindrical or spherical gas bubble. Owing to this claims the ideal gas law, the energy, the momentum and continuity equation must be solved coupled. For the aimed analytical solution, the set of equations which are dependent on time and place are linearised. Furthermore a separation ansatz eliminates the time dependence. Two ordinary coupled differential equations remain resulting in an eigenvalue problem. So far the treatment is pure analytical for all coordinate systems. This approach has origin from the analysis of the dynamic behavior of air springs (*Pelz & Buttenbender (2004)*. Interestingly an air-spring can be considered as an up-scaled cavitation bubble. The cut-of frequency were the transition from isothermal to adiabatic compression happens of a typical passenger car air spring is of the order $\omega_\gamma /(2\pi) \sim 0.01$ Hz. The cut off-frequency at which the change from isothermal to isentropic compression happens to be is determined by the balance between change of inner energy during a half cycle and the heat transport rate over the boundary of the bubble, air spring respectively. Hence the cut-

off frequency is of the form $\omega_\gamma = \dfrac{j+1}{r_0} \dfrac{k}{c_p \rho_0} f(\kappa, \gamma)$ were the volume specific area of the bubble is given by $(j+1)/r_0$ for the plane ($j=0$), cylindrical ($j=1$) and spherical ($j=2$) bubble respectively. The heat transfer coefficient is denoted by k, the specific heat is c_p, the density ρ_0 and the isentropic exponent γ (=7/5 for a diatomic gas). Here and in the following the geometry, state, and material variables at rest are denoted by the subscript 0. For small bubbles with $\kappa := r_0 a_0 / D_0 < 10$ the travelling time of a sound wave through the air volume r_0 / a_0 is of the order of the thermal diffusion time r_0^2 / D_0 with the thermal diffusivity $D_0 = \lambda / \rho_0 c_p$ (heat conductivity λ, sound speed $a_0 = \sqrt{\gamma R T_0}$, isentropic exponent $\gamma = 7/5$ for diatomic gas, gas constant R). For an air spring or a "big" bubble κ is much greater than 10. Hence the cut-off frequency scales as $\omega_\gamma \sim (j+1)/r_0$. The typical length of an air spring is 0.1 m, the typical size of a cavitation bubble is 1 μm. Hence there is a scaling factor of 10^5 for the cut-off frequency, which is above 1 kHz for a cavitation bubble. This fits to the cut-off frequency of 0.01 Hz for the vehicle air-spring[1].

Considering the equation of motion for a cavitation bubble, the Rayleigh-Plesset equation without viscous damping and diffusion reads as:

$$p_B - p_\infty = \rho_l \ddot{R} R + \frac{3}{2} \rho_l \dot{R}^2 + \frac{2S}{R},$$

with the pressure at the interior side of the bubble wall p_B, the pressure at infinity p_∞, the liquid density ρ_l, coefficient of surface tension S and bubble radius $R(t)$. In a perturbation analysis with $R = r_0(1 + h_+)$ considering only linear terms in h_+ we end up for the spherical case with the characteristic equation

$$0 = -\omega_0^2 + \frac{3 K_+(\omega_0) p_0}{\rho_l r_0^2} - \frac{2S}{\rho_l r_0^3}.$$

It is emphasized that the compression modulus changes with the frequency. By gaining the equation we have linearized p_B using the complex compression moduls $K_+(Pe, \kappa)$ (Equation

---

[1] On has to be carefully with the given scaling result, since if the cut-off frequency is dependent on $\omega_\gamma = f(r_0, a_0, D_0, \gamma)$ the dimensional analysis would results in $\omega_\gamma r_0^2 / D_0 = f(\kappa, \gamma)$, which is accordance with the boundary value problem (3) and a scaling law of $\omega_\gamma \sim r_0^{-2}$ would result for "big" bubbles.

(7), Figures 2, 4). The dependence of the compression modulus on frequency is the main task of the presented work.
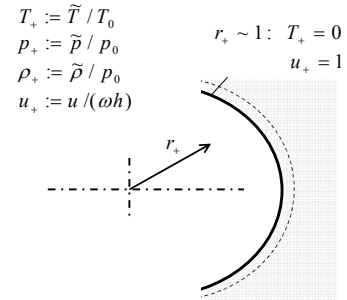
We do not take the heat conduction within the liquid into account. This would result in an additional typical time scale, i.e. the temperature diffusion time within the liquid. Since this time is much smaller compared with the diffusion time within the gas, it is not considered here.

THEORETICAL, ANALYTIC APPROACH
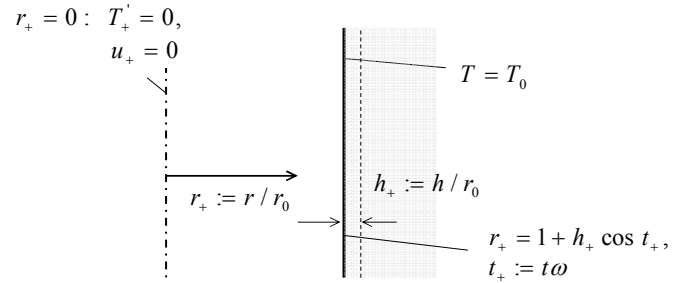
Figure 1: Geometry and boundary conditions for (i) the plane and cylindrical bubble, (ii) the spherical bubble.

The analytic, numerical examination takes place in two steps. In the first place the conservation laws are solved for the plane case. The thought experiment consists of two half infinity plates with a gas filled gap. Due to symmetry the midplane is adiabatic and fixed. The bubble boundary has a constant temperature, i.e. the thermal diffusion time in the water is assumed to be much smaller than the attenuation time $2\pi / \omega$ due to the forced harmonic oscillation of the bubble boundary $r_+ = 1 + h_+ \cos(\omega t)$. (The spatial coordinate $r = r_+ r_0$ and the amplitude $h = h_+ r_0$ are measured with the typical length of the gas volume. The time is measured by $1/\omega$: $t = t_+ / \omega$.) In a second step the examinations are enlarged on cylindrical and spherical geometry.

To derive the coupled linearized differential equations to be solved a perturbation ansatz is used in the ideal gas law, the continuity, the momentum and the energy equation:

$$p = \rho RT,$$

$$\frac{D\rho}{Dt} + \rho \nabla \cdot \vec{u} = 0,$$

$$\rho \frac{D\vec{u}}{Dt} = \nabla \cdot \overline{T}, \text{ with} \tag{1}$$

$$\overline{T} = \mu(\nabla \vec{u} + \nabla \vec{u}^T) + [(\mu_d - 2\mu/3)\nabla \cdot \vec{u} - p]\overline{I},$$

$$\rho c_v \frac{DT}{Dt} - \frac{p}{\rho}\frac{D\rho}{Dt} = \Phi + \nabla \cdot (\lambda \nabla T).$$

Here Φ is the dissipation function, p the pressure, $\vec{u} = u\vec{e}_r$ the velocity vector, which has for the assumed one-dimensional case only a component in the normal direction of the bubble wall, μ the dynamic and μ_d the pressure viscosity of the gas. For the one dimensional case there appears only the combination $\hat{\mu} = 4\mu/3 + \mu_d$ and is made dimensionless in form of the Prandtl number $\text{Pr} := \hat{\mu}/(\rho_0 D_0)$. For vanishing pressure viscosity the Prandtl number is determined by $\text{Pr} = [4\gamma/(9\gamma - 5)]4/3 = 7/10$ for a diatomic gas, which is assumed here for all results shown in the following figures. For a non vanishing pressure viscosity the results are gained in the very same way.

The system (1) becomes linear, if only small perturbations are considered. The ansatz

$$p = p_0 + \widetilde{p},$$
$$T = T_0 + \widetilde{T} = T_0 + T_0\theta(r_+)e^{it_+},$$
$$\rho = \rho_0 + \widetilde{\rho}, \tag{2}$$
$$u = \widetilde{u} = i\omega h\varphi(r_+)e^{it_+}$$

($i = \sqrt{-1}$) leads to two coupled differential equations for all three considered geometric cases for the plane, cylindrical and spherical bubble. By introducing the number $j=0$ for the plane, $j=1$ for the cylindrical and $j=2$ spherical bubble, the boundary value problem for the velocity amplitude $\varphi(r_+)$ and temperature amplitude $\theta(r_+)$ reads in a comprehensive form as:

$$\theta(r_+) + h_+(\gamma - 1)\left[\varphi'(r_+) + \frac{j}{r_+}\varphi(r_+)\right] +$$

$$+ i\frac{\gamma}{\text{Pe}}\left[\theta''(r_+) + \frac{j}{r_+}\theta'(r_+)\right] = 0,$$

$$\gamma \text{Pe}^2\varphi(r_+) - \frac{\kappa^2}{h_+}\theta'(r_+) + \tag{3}$$

$$+ \left(\kappa^2 + \frac{4}{3}i\gamma \text{Pr Pe}\right)\left[\varphi''(r_+) + \frac{j}{r_+}\varphi'(r_+) - \frac{j}{r_+^2}\varphi(r_+)\right] = 0,$$

$$\varphi(0) = 0, \quad \theta'(0) = 0,$$
$$\varphi(1) = 1, \quad \theta(1) = 0.$$

The boundary value problem (3) is merely dependent on the isentropic exponent γ, the Péclet number or dimensionless attenuation frequency $\text{Pe} = \omega r_0^2/D_0$ were the cycle time is measured with the thermal diffusion time r_0^2/D_0, the Prandtl number Pr, the already introduced dimensionless length $\kappa = r_0 a_0/D_0$ and the dimensionless oscillation amplitude $h^+ = h/r_0$. For convenience the spatial derivative is written as prime. As it was said the dimensionless canal height κ can be considered to be the ratio of a temperature diffusion time r_0^2/D divided by the travel time r_0/a_0 of a pressure wave. For small $\kappa < 10$ the diffusion time is of the order of the running time of the pressure wave. That accounts for the observed different behavior of the solution for this parameter value range.

During the analytic analysis of these differential equations the eigenvalues λ_k and corresponding eigenvectors $c_{1,k}$ and $c_{2,k}$ assume the form

$$\lambda_k = \pm \sqrt{\frac{i\kappa^2 - \frac{4}{3}\text{PrPe} - \gamma\text{Pe} \pm \sqrt{\left[\left(\frac{4}{3}\text{Pr} + \gamma\right)\text{Pe} - i\kappa^2\right]^2 + 4i\text{Pe}^2\left(\frac{4}{3}i\gamma\text{Pr} + \frac{\kappa^2}{\text{Pe}}\right)}}{\frac{8}{3}i\gamma\text{Pr} + 2\frac{\kappa^2}{\text{Pe}}}}$$

$$\tag{4}$$

$$c_{1,k} = \frac{\gamma\lambda_k^2 - i\,\text{Pe}}{i(\gamma - 1)h_+\lambda_k\,\text{Pe}}, \quad c_{2,k} = 1, \text{ with } k = 1,...,4.$$

Hence the analytic solution is

$$\begin{pmatrix}\varphi \\ \theta\end{pmatrix} = \sum_{k=1}^{4} a_k \begin{pmatrix}c_{1,k} \\ c_{2,k}\end{pmatrix} e^{\lambda_k r_+}, \tag{5}$$

whereas the constants a_k are determined by the boundary conditions. To verify whether the behavior of the general solution is isothermal or isentropic the plane equations were also solved with the following assumptions. For the isentropic case $\hat{\mu} = \lambda = 0$ were set to zero so that friction and heat conductivity were removed. In the isothermal case the perturbation of temperature $\widetilde{T} = 0$ were set to zero.

RESULTS
The solutions of the current investigation are the complete state variables and the velocity of the gas inside the bubble for plane, cylindrical and spherical bubble ($j=0,1,2$). Since doe to the linearity of the boundary value problem (3) the results are proportional to the attenuation amplitude. Hence, it is convenient to introduce a transfer function k_+ between dimensionless oscillation amplitude h_+ as input signal and the dimensionless pressure p_+ as output signal:

$$k_+(r_+) := \frac{1}{j+1}\left|\frac{p_+}{h_+}\right| = \frac{1}{j+1}\left|\frac{\theta(r_+)}{h_+} - \left(\varphi'(r_+) + \frac{j}{r_+}\varphi(r_+)\right)\right| \tag{6}$$

The frequency response characteristic is a complex function. As result outcomes the value and the phase of the propagation. For a multi phase flow the compression modulus of the bubble is of

(i)
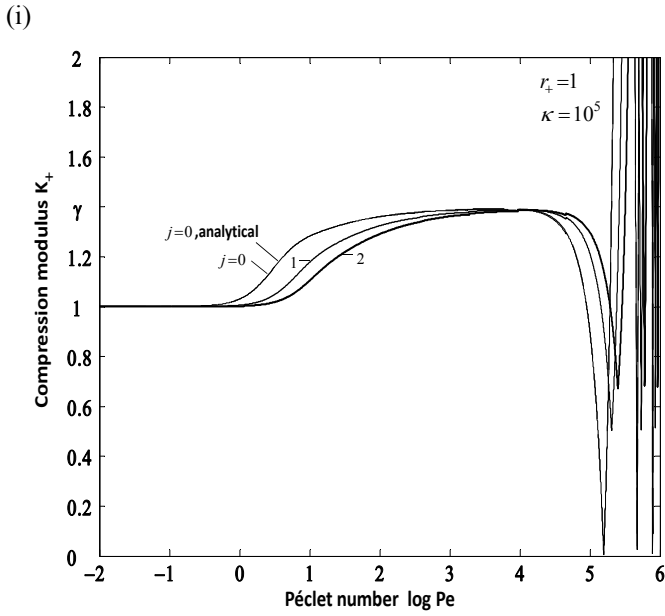
(ii) using the volume specific surface as typical length
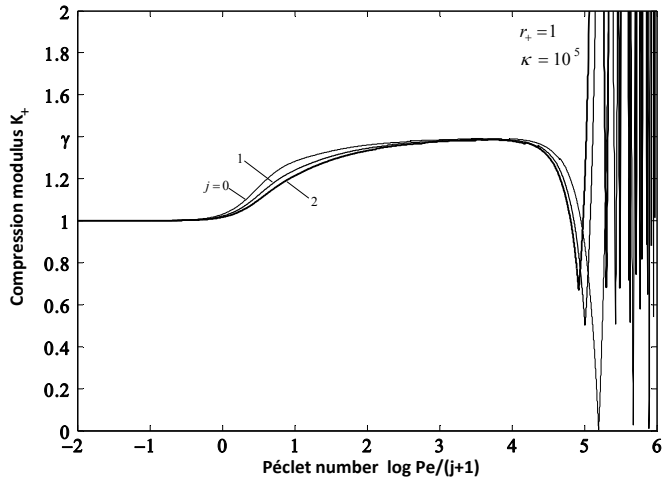
Figure 2: Compression modulus K_+ for the plane case $j=0$ numerical and analytical, cylindrical case $j=1$ and the spherical case $j=2$ numerical (i) over Pe and (ii) over Pe/(j+1) (with the volume specific surface as typical length). All for $\gamma=7/5$, high $\kappa=10^5$
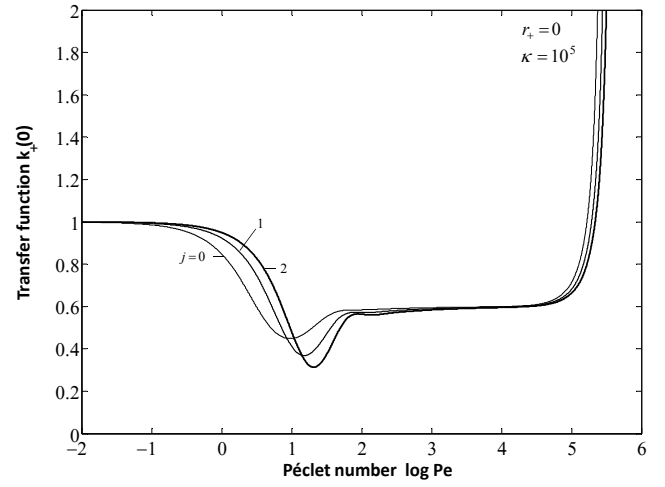
Figure 3: Transfer function at the fixed point $r_+=0$ for the plane case $j=0$, the cylindrical case $j=1$ and the spherical case $j=2$ over Pe. All for $\gamma=7/5$, high $\kappa=10^5$.
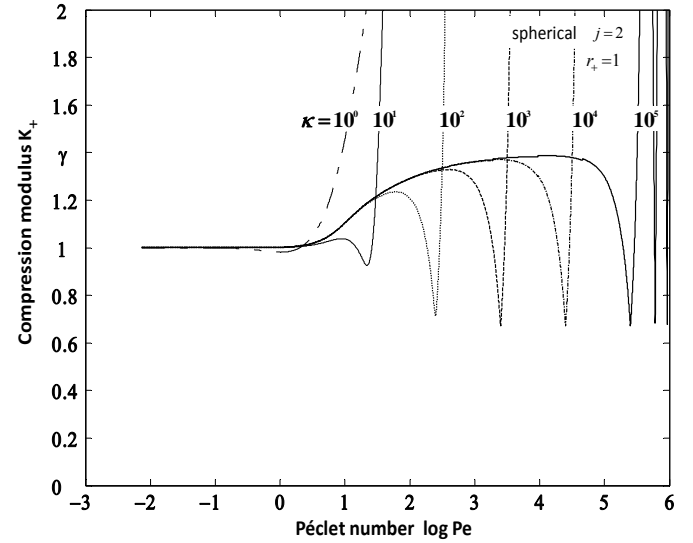
Figure 4: Compression modulus K_+ for the spherical case $j=3$ over Pe with varying dimensionless length κ ($\gamma=7/5$).

4
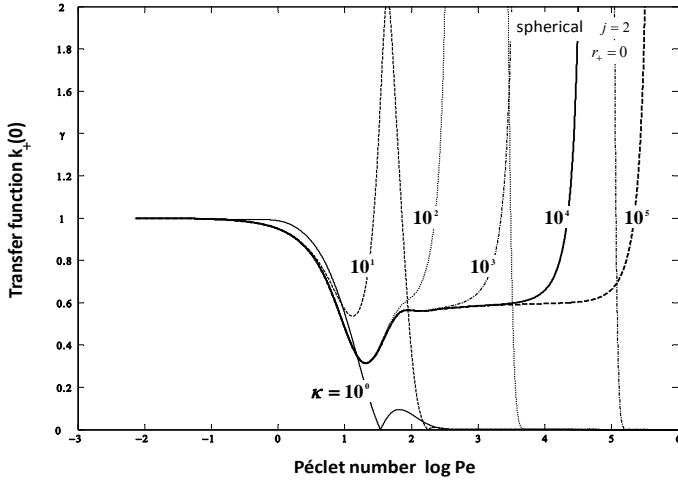
Figure 5: Transfer function at the fixed point $r_+=0$ for the spherical case $j=3$ over Pe with varying dimensionless length κ. ($\gamma=7/5$).

importance. It is defined as pressure change with volume change $K := -V dp/dV$, which assumes the dimensionless form for the plane, cylindrical and spherical case is the boundary value of equation (6):

$$K_+ := k_+(r_+=1).\qquad(7)$$

In the following figures 2 to 5 the transfer functions are plotted for variable parameters. In figure 2 the compression modulus is outlined over the Péclet number and the shape parameter j for high dimensionless typical length $\kappa=1e5$. Figure 3 displays the transfer function evaluated at the plane/line/point of symmetry $r_+=0$ for different j and the same κ. Figure 4 and 5 show the same only for decreasing κ and spherical geometry $j=2$.

In figure 2 the compression modulus assumes the constant asymptotic value of $K_+=1$ for low Pe and shows as expected the isothermal behavior for all cases. After the transient area that offsets to higher Pe with advancing j a second plateau is apprenticed that behaves isentropic with an absolute value $K_+=\gamma$ as expected.

The shift of the cut-off frequency to higher Péclet numbers is well explained by the difference in the volume specific surface area of the bubbles. As it was shown in the introduction, the cut-off frequency and hence the Péclet number scales as $\mathrm{Pe}_\gamma \sim \beta$. Indeed there is a shift of ~6 between $j=2$ and $j=0$ and a shift of ~4 between $j=1$ and $j=0$ as it is expected from the dimensional analysis. Increasing the frequency and hence the Peclet number it comes to an oscillation which also behaves like the calculated isentropic case. The oscillations also offset to higher Pe. Furthermore the minima have greater values with advancing j and as well for advancing Pe. It is interesting, that the extremes in the analytical plane case appear in dependence to the dimensionless length κ. For the zero singularity with the
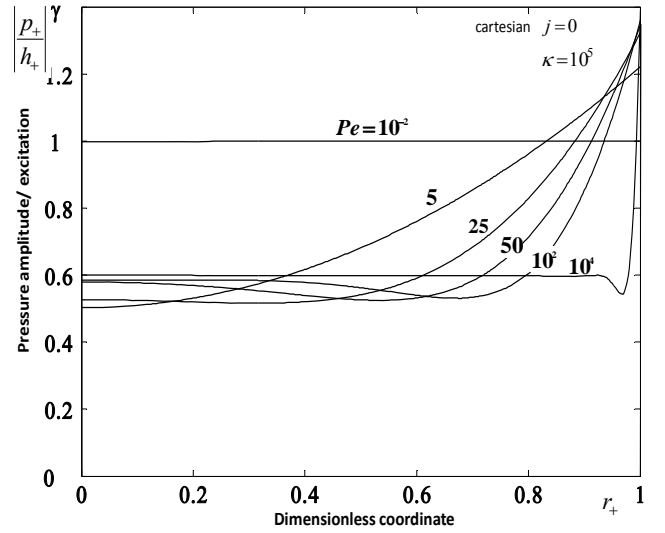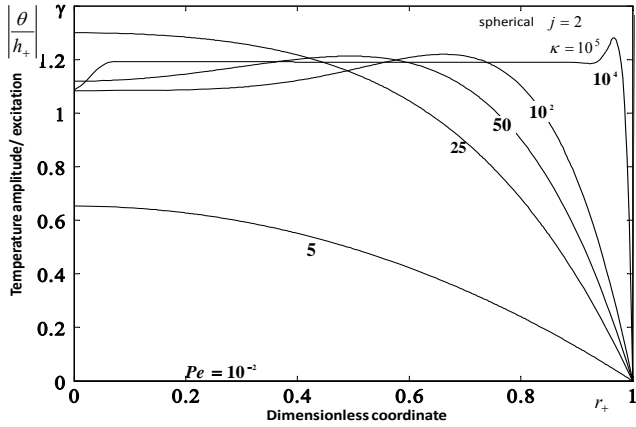

Figure 6: Spatial pressure distribution p_+ divided by excitation h_+ for the plane case $j=0$, for $\gamma=7/5$, high $\kappa=10^5$ and low Pe.
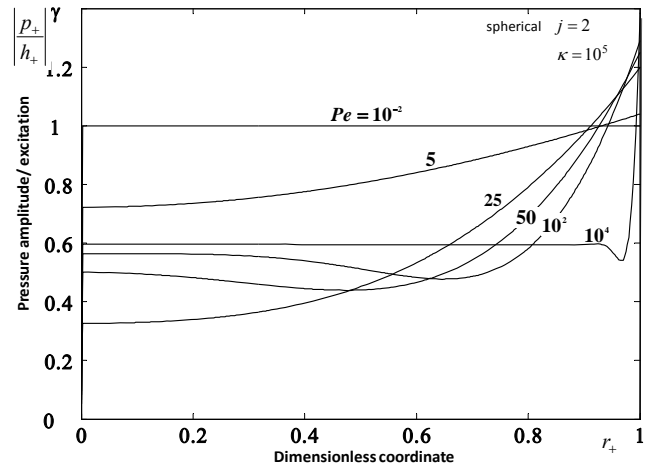
Figure 7: Spatial pressure distribution p_+ divided by excitation h_+ for the spherical case $j=2$, for $\gamma=7/5$, high $\kappa=10^5$ and low Pe .
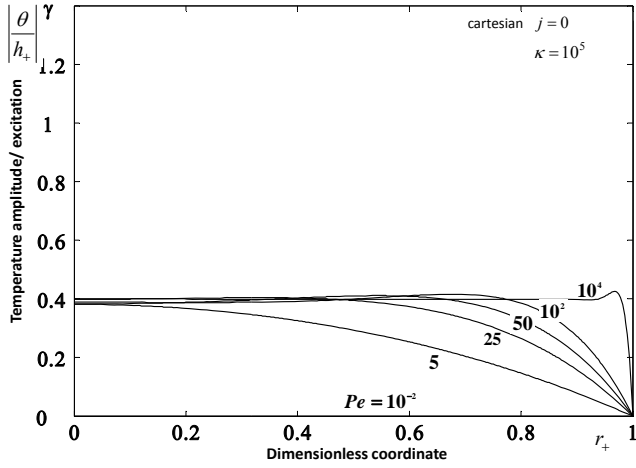
Figure 8: Spatial temperature distribution θ divided by excitation h_+ for the plane case $j=0$, for $\gamma=7/5$, high $\kappa=10^5$ and low Pe.

Figure 9: Spatial temperature distribution θ divided by excitation h_+ for the spherical case $j=2$, for $\gamma=7/5$, high $\kappa=10^5$ and low Pe .

prefactor $\pi/2$ and for the infinite singularity with π. This behavior is explained by the detailed analytical solution.

At Pe = $(\pi/2, 3/2\pi,...)\kappa$ a standing pressure wave with the node at the wall is observed. For Pe = $(\pi, 2\pi,...)\kappa$ the node is in the center. It is assumed that a similar relation in the form Pe = $(\alpha\pi/2, 3\alpha/2\pi,...)\kappa$ and Pe = $(\alpha\pi, 2\alpha\pi,...)\kappa$ can be given for the cylindrical and spherical case but due to mere numerical results the shift factor α cannot be given exactly. For example it varies between $\alpha=1.2...1.6$ for $j=2$. After the region of oscillations a second area with isothermal behavior is proven for the analytical plane case for Péclet numbers of the order Pe$\approx\kappa^2$.

In figure 3 the transfer function is evaluated at the symmetry point $r_+=0$. With low Péclet numbers it likewise has a plateau value *1* what is expected because at very low frequencies the pressure is spatially constant. Thereafter again a transition area appears that leads to a minimum before a second plateau

develops. Here also the transient areas offset to higher Péclet numbers with increasing j and also the minima show lower values. Following the second plateau the transfer function strives to infinity.

The figures 4 and 5 reveal the dependence of the transfer function and especially of the compression modulus on the dimensionless length κ. For all κ in both cases for $r_+=1$ and $r_+=0$ the first isothermal plateau stays unaltered. The transition area obtains a larger range for $r_+=1$and stays almost unchanged for $r_+=0$. The second isentropic plateau grows in either instance in length with increasing κ. Moreover the oscillation ($r_+=1$) striving to infinity ($r_+=0$) is shoved to higher Péclet numbers. The behavior for lower $\kappa <10$ is slightly different. Here, too the first sections of the curves are quite similar but at the beginning of the transition area the developing changes increasing with decreasing κ. Especially for very low $\kappa\sim1$ the development of the graph gets complete different and is not understood yet but a reason could be that in this region the temperature diffusion time r_0^2/D and the travel time r_0/a_0 of a pressure wave are of the same order. There, compared with the analytic isothermal solution, only isothermal behavior is shown. However at this point concerns must be risen because such low κ imply a typical lenth of *100nm*. An infinite stiffness would result.

Following the spatial pressure and temperature distributions divided by h_+ for the plane and the spherical case are brought face to face. Therefore first the courses for low Péclet numbers will be discussed up to the end of the transition area. Afterwards the distributions for the maxima and minima, shown in figure 1, are considered.

Figures 6 and 8 illustrate the dimensionless pressure amplitude p_+ and temperature amplitude θ both divided by h_+ over the dimensionless length r_+, for the plane case. For low Péclet numbers the pressure and temperature is constant over the whole region. This is in figure 2 and 3 the plateau that assumes the value one and behaves isothermal. With rising Péclet number the pressure amplitude at the plane of symmetry decreases to a minimum value before the second plateau is accomplished. This is the transition area in figure 3. Meanwhile the pressure at the oscillating wall rises from one thru the transition area in figure 2 to the value of the isentropic exponent γ. Thereby the boundary layer thickness decreases towards the moving wall. Due to the fact that the solution for the pressure is composed of one part with the first derivative of the velocity and another part consisting of the temperature (see eq. 6) there is a connection between the pressure and the temperature amplitude except for $r_+=1$, there the boundary condition is a constant temperature.

The temperature amplitude shown in figure 8 rises on the fixed adiabatic plane of symmetry from the spatial constant value of zero for low Péclet numbers to a plateau which has due to the boundary conditions no gradient at $r_+\rightarrow0$. The boundary layer too decreases. In doing so the gradient at the oscillation wall increases due to the fact that the amplitude at the wall with constant temperature must be zero. The influence on the pressure amplitude at the moving wall declines ever steeply with higher dimensionless frequencies *Pe*. It is fact that the pressure amplitude at the oscillating wall is only influenced by the first derivative of the speed (eq. 6). For the other cases this

Figures 8 and 9 show the same courses for the spherical case *j=2*. Basically the distributions show the same behavior is different.
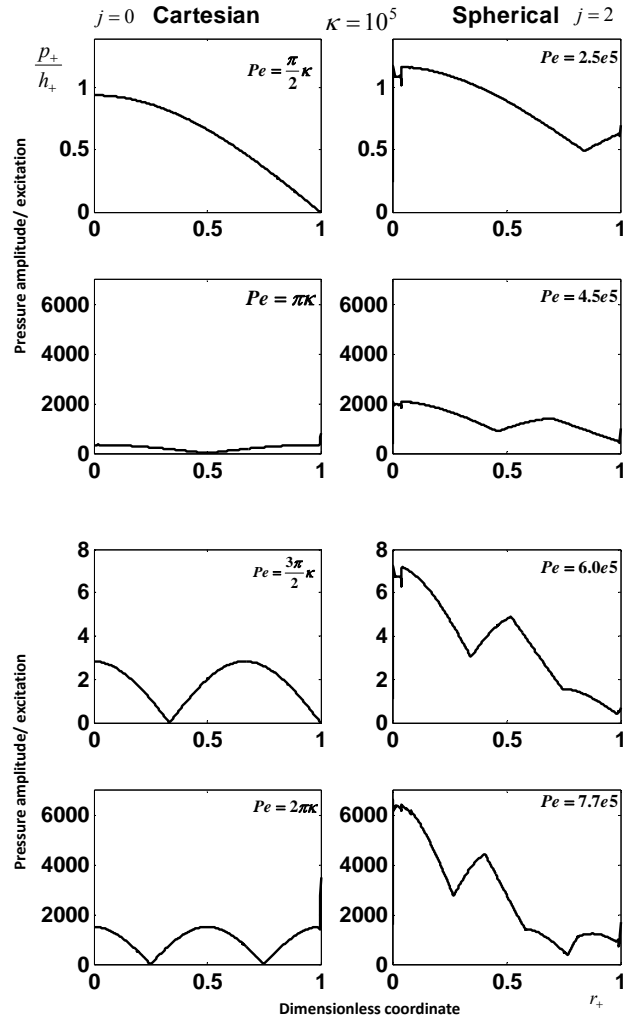
Figure 10: Spatial pressure distribution p_+ divided by excitation h_+ for the plane case *j=0* on the left column and for the spherical case *j=2* on the right. First row shows the first minimum, second row the first maximum. Followed by the second minimum and the second maximum. All plotted for *γ=7/5,* high *κ=10⁵* .

The center point the value of the pressure amplitude also decreases from a constant value of one to a this time lower minimum, then rises again to the same plateau value. This was already pointed out in figure 3. On the oscillating wall the pressure amplitude rises again from the value 1 to *γ.*
All this is displaced to higher Péclet numbers as shown in figure 2 and 3. The temperature amplitude has greater values as in the plane case but likewise the boundary thickness decreases with rising Péclet numbers and the declination to zero is even steeper. This slightly different behavior is probably a result of

the additional terms j/r and j/r^2 which appear in the spherical and cylindrical case. The cylindrical case has the same courses and lies between the plane and spherical case. Up next the spatial pressure courses for the extremes in figure 2 will be considered for the plane and spherical case. The plots for the first two minima and maxima are shown in figure 10. On the left side the plane case is placed. The first minimum appears at Pe=πκ/2 calculated analytical. This standing wave has its node with the value of zero at $r_+=1$ as expected from figure 1. Following the minimum a maximum develops for Pe=πκ with high values for the pressure amplitude at the plane of symmetry and at the oscillating wall. In the middle of the region resides the node of the standing wave with the value zero. The next two images show the second minima and maxima. With every new extremum an additive node appears in the standing wave. Moreover with every extremum of the transfer function the maxima of the standing wave rise to higher values. The same can be said for the distribution of the temperature amplitude. Only the absolute values vary but the courses are completely the same for the plane case. General the minima develop at Pe = *(π/2, 3/2π,...)κ* and the maxima at Pe = *(π, 2π,...)κ.* For the analytical and numerical solution there is a discontinuity at the boundary due to the boundary condition. It is worthwhile to consider also the surrounding fluid as it was done before by Prosperetti. For the spherical case the results are different. There the nodes do not reach the value zero and when the minimum in the frequency response characteristic is developed the node is not at the oscillating wall but it has moved a bid further towards the center. It is assumed that this comes from discretisation errors produced by solving the equations with FE methods. The standing wave does not show such a regular behavior as in the plane case. Its maximums have the highest values at the center point. From there the pressure amplitude decreases to the point of the node and then rises again but to a this time lower maximum. The temperature amplitude has not the similar characteristic as in the plane case. It has nodes with the worth zero which are displaced related to the pressure ones. Despite these peculiar properties it is apparent that the pressure amplitude gets higher values for each extremum in the transfer function, even significant higher ones as in the plane case.

DISCUSSION

In this work the compression modulus as a function of the dimensionless frequency Pe and the dimensionless length *κ* is explained by solving the conservation laws for the gas within a plane, cylindrical and spherical bubble. The special distributions of pressure and temperature within the bubble give a clear picture of standing pressure and temperature waves. A critical parameter in doing so is *κ* which can be looked at as the ratio of a temperature diffusion time r_0^2/D divided by the travel time r_0/a_0 of a pressure wave. For low *κ* the diffusion time is of the order of the running time of the pressure wave.

$$\kappa \gg 10: \quad \frac{r_0^2}{D_0} \gg \frac{r_0}{a_0}$$

$$\kappa \sim 1...10: \quad \frac{r_0^2}{D_0} \sim \frac{r_0}{a_0} \qquad (8)$$

Hence an isothermal behavior is reasonable and indeed observed in the analysis for low κ. If this is the case for high Pe can not be judged. Further investigations can for example modify the temperature boundary condition at the oscillating wall taking the temperature diffusion within the surrounding water into account.

$$\log \kappa = \log \frac{r_0 a_0}{D_0}$$
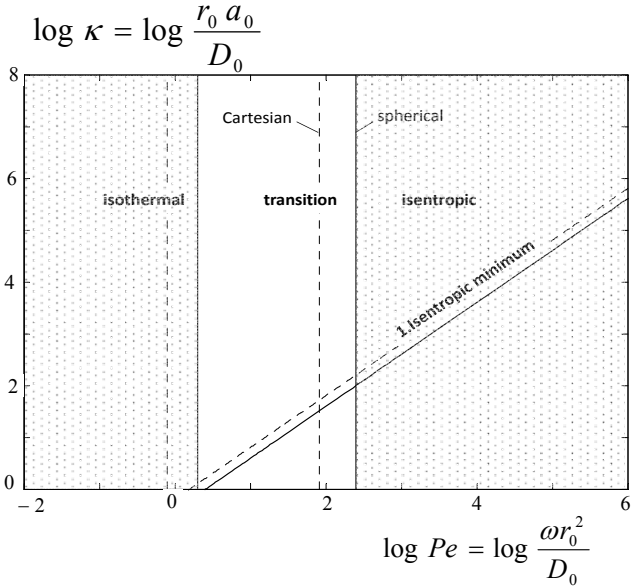
Figure 11: Parameter map for the solution of the boundary value problem (eqn. 3) for $\gamma=7/5$.

The difference between plane, cylindrical and spherical bubbles is explained by the difference in the dimensionless volume specific surface area (see also the parameter map in figure 11). The dimensional analysis done in the introduction is very well capable to explain the observed shift in the cut-off frequency qualitative and quantitative. As it was shown by *Pelz & Buttenbender* [3] matching the solution of the boundary value problem (eq. 3) with a solution gained for homogeneous thermodynamic state $K_+ = |i\gamma \text{ Nu}/\text{Pe} - \gamma| / |-i\gamma \text{ Nu}/\text{Pe} + 1|$ within the gas volume the Nusselt number is determined by $\text{Nu} := kr_0 / \beta\lambda \sim 3$. This again confirms the above given scaling law (see figure 12).
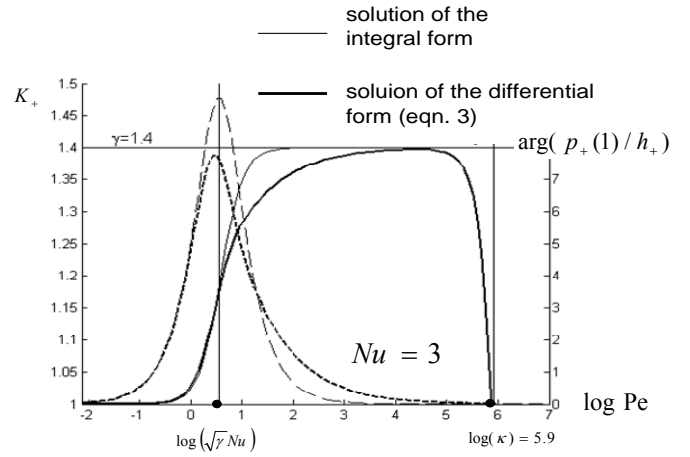
Figure 12: Compression modulus for homogeneous thermodynamic state [3] for a Nusselt number of 3 and the solution of eq. 3 for j=0, $\gamma=7/5$ and high $\kappa=10^{5.9}$.

CONCLUSION

Extending previous works on bubble dynamics by Prosperetti and on the first glance far away working areas like dynamic behavior of air springs in vehicle dynamics a scaling law for the cut-off frequency of an air spring is derived. The scaling law takes the bubble shape and the bubble size into account. Up to now the limiting case, were the thermal diffusion time is of the order of the wage traveling time, has not been considered close. Interestingly for such small bubbles there is no transition between isothermal and isentropic compression even at high frequencies.

NOMENCLATURE

a_0 : speed of sound
c_p : specific heat capacity
D : thermal diffusity
h : oscillation amplitude
h_+ : dimensionless oscillation amplitude
i : root of minus one
j : geometry parameter 0,1,2
k : heat transfer coefficient
k_+ : transfer function
K : compression modulus
K_+ : dimensionless compression modulus
p : pressure
p_0 : constant pressure
$\tilde{p}$: pressure disturbance
p_B : pressure interior side of the bubble wall
p_+ : place dependant dimensionless pressure amplitude
Pe : Péclet number
Pr : Prandtl number
r_0 : constant radius/canal height
r_+ : dimensionless coordinate
R : gas constant, Bubble Radius
S : coefficient surface tension
t : time
t_+ : dimensionless time
T : temperature
T_0 : constant temperature
$\tilde{T}$: temperature disturbance
u : velocity
$\tilde{u}$: velocity disturbance
V : volume

α : geometry factor
β : geometry factor for the volume specific area
φ : place dependent velocity amplitude
Φ : dissipation function
γ : isentropic exponent

λ : heat conductivity, eigenvalue
μ : dynamic viscosity
κ : dimensionless length
ω : oscillation frequency
ω_0 : eigenvalue
$\omega \gamma$: cut-off frequency
ρ : density
ρ_0 : constant density
ρ_l : liquid density
$\tilde{\rho}$: density disturbance
θ : place dependent temperature amplitude

D/Dt : substantial time derivative
$(\dot{\ })$: partial time derivative
$(\ )'$: partial spatial derivative

REFERENCES

[1] Plesset & Prosperetti 1977 ; Bubble dynamics and cavitation; Ann. Rev. Fluid Mech 1977; 9 : 145-85
[2] Feng & Leal 1997 ; Nonlinear bubble dynamics; Ann. Rev. Fluid Mech 1997; 29 :201-43
[3] Pelz & Buttenbender 2004 ; The dynamic stiffness of an air-spring; ISMA 2004 International Conference on Noise & Vibration Engineering
[4] Prosperetti 1991 ; The thermal behavior of oscillating gas bubbles , J. Fluid Mech. (1991) vol. 222, pp. 587-616